http://dx.doi.org/10.1016/j.energy.2023.130042

Day-ahead schedule optimization of household appliances for demand flexibility: case study on PV/T powered buildings

Chuyao Wang [1 *], Jie Ji [2], Hongxing Yang [1].

[1]Renewable Energy Research Group (RERG), Department of Building Environment and Energy Engineering, The Hong Kong Polytechnic University, Hong Kong, China

[2]Department of Thermal Science and Energy Engineering, University of Science and Technology of China, Hefei, China

Abstract

Employing the demand flexibility strategy in PV powered buildings can effectively balance solar energy supply and building energy demand, thereby increasing the self-consumption ratio of PV electricity. Despite this, its solar energy utilization is still low due to the limit of the PV efficiency. On the other hand, PV/T modules not only generate electricity but also produce domestic hot water, thus providing higher solar efficiency. In this study, the demand flexibility of various shiftable appliances in a PV/T powered building was investigated. An optimization-based demand flexibility strategy was proposed to reduce electricity cost and maximum grid power. The case study showed that the proposed strategy could reduce the electricity cost by 23% and smooth grid power fluctuation. Moreover, compared with the PV powered building, the PV/T powered building could reduce the electricity cost by 10% and significantly improve utility grid friendliness. Furthermore, the forecast error of boundary conditions negatively affected the electricity cost and grid power fluctuations. The sensitivity analysis revealed that the ambient temperature and solar irradiation on the PV/T modules had a greater impact on the optimization objective. Overall, this work aims to provide guidance for planning the flexibility operation of PV/T powered buildings.

Keywords: Demand flexibility; Building appliances; PV/T module; Global optimization; MILP.

Nomenclature

Abbreviation

PV/T photovoltaic/thermal

MILP mixed integer linear program

EV electric vehicle

WM washing machine

DW dishwasher

EWH electric water heater

Symbol

P electricity power (W)

Q heat power (W)

G solar radiation (W)

T temperature (°C)

U heat transfer coefficient ($W \cdot m^{-2} \cdot K^{-1}$)

A area (m^2)

F_R heat remove factor

τ solar transmittance

α solar absorptivity

η efficiency

R thermal resistance ($W^{-1} \cdot m^2 \cdot K$)

β_r temperature coefficient (K^{-1})

C heat capacity ($J \cdot K^{-1}$)

S heat stored (J)

γ binary variable

Subscript

a room air

m massive wall

w window

in inner surface

out outer surface

s PV/T modules

e wet appliance

v electric vehicles

o non-shiftable appliances

g utility grid

t water tank

p absorber plate

amb ambient air

tar water tank target temperature

eva water evaporation temperature

loss heat loss of water tank

1

2

1. Introduction

With the rapid development of urban modernization, energy consumption in buildings is gradually becoming the primary source of global energy use. Relevant data shows that building operations account for 30% of final energy consumption and 27% of total carbon emissions [1]. The operation of building appliances depends on many factors, such as weather, human activity, and other variables, rendering it highly stochastic [2]. Inadequate planning of building operations may result in an imbalance between grid power supply and building energy demand. This not only hampers cost reduction for customers but also poses a threat to grid stability. Building energy flexibility is a popular demand side management strategy for balancing supply and demand. It utilizes the load-shiftable characteristics of some household appliances to reconfigure the building demand profiles [3]. The shiftable appliances include the HVAC system, electricity water heater, wet appliances, and electricity storage device et al. The power and operation hours of these devices can be adjusted to provide demand response service without sacrificing user comfort. Over the years, many studies on the flexibility operation of building appliances have been conducted.

1.1 Literature review

The HVAC system is the largest energy consumer in the building, accounting for 40-60% of total energy consumption [4]. The heat charging and discharging of the building's thermal mass (i.e., massive wall and interior furniture et al.) is the primary resource for providing demand flexibility to HVAC systems [5]. Typically, air-conditioning loads are modulated through temperature set-point resetting and pre-cooling/pre-heating [6]. Dreau et al. [7] and Foteinaki et al. [8] modulated the heating power of two residential buildings by decreasing and increasing the temperature set point. It was concluded that the energy cost could be reduced and the peaking power was removed. Chen et al. [9] conducted an experiment to investigate the load reduction potential by temperature reset and pre-cooling. They found that the indoor thermal mass and active energy storage could achieve the demand response in the short and long term, respectively. Liu et al. [10] proposed a temperature-reset method considering the future weather conditions and electricity prices for shifting the energy demand. Troitzsch et al. [11] developed a mixed-integer quadratic program to plan the electric

distribution grid incorporating demand-side flexibility from thermal building systems. Fan et al. [12] used the Wildebeest Herd Optimization algorithm to improve the demand for thermostat settings. Ding et al. [13] proposed a dual-objective coordinated optimization approach, which optimized the temperature set points of the office building while considering the forecast uncertainty.

The electric water heater is another energy flexibility resource in household appliances. Compared to other household appliances, electric water heaters have the highest rate power and significant thermal storage capacity [14]. The electricity consumed by water heaters can be stored in the form of heat and then utilized at other times to respond to utility grid demands [15]. Kepplinger et al. [16] developed a binary integer program to plan the operation of the electric water heater. Compared with the conventional night tariff-switched operation, the cost saving and energy saving were respectively 12% and 4%. Khalid et al. [17] controlled the operation of the electric water heater based on the Q-learning and dynamic programming method. Lin et al. [18] developed a grey-box model for predicting hot water loads and then proposed a genetic algorithm to optimize the operation of electric water heaters. Wang et al. [19] planned the operation of the electric water heater using the robust optimization, considering uncertainty factors of boundary conditions. Gómez et al. [20] proposed an energy management system for electric water heater to minimize operation costs without compromising the comfort. The strategy was programmed in the computer operating system to drive realistic operation. Kapsalis et al. [21] scheduled the operation of electric water heaters using the heuristic algorithm, considering both the objectives of energy cost and user comfort.

In addition to the above-mentioned thermostatically controlled appliances, some postponable appliances, such as washing machines, dishwashers, and chargers, can also provide the energy flexibility [22]. These appliances respond to grid demand by scheduling their running time within a flexibility window [23]. Klaassen et al. [24] evaluated the flexibility potential of the residential appliances under the dynamic tariff. It was concluded that the effective and transparent tariff was crucial for the demand response of these appliances. Lezama et al. [25] formulated the aggregator appliances management as a Mixed-Integer Non-Linear Program problem. D'hulst et al. [23] estimated the demand response flexibility of residential smart appliances based on the pilot test. The flexibility potential of wet appliances in Belgium was explored. Setlhaolo et al. [26] studied the scheduling of typical home appliances using the mixed integer nonlinear optimization model. Their

case study showed that the electricity cost savings of over 25% were achieved.

With the increasing penetration of solar technology in buildings, the application of PV modules on buildings to supply electricity for household appliances is becoming an important way of building energy saving [27]. However, several critical issues arise due to the mismatch between the PV power supply and building load. Firstly, PV systems generate electricity based on sunlight availability, leading to intermittent power generation. This poses challenges in maintaining a stable power supply and may result in a low self-consumption ratio. Secondly, the fluctuating nature of PV power injection can impact the stability of the power grid, potentially causing voltage and frequency deviations. Although employing batteries can mitigate the impacts of intermittent PV generation on the utility grid, their high initial investment limits practical implementation. The use of demand flexibility strategies proves to be an economic and effective method to balance PV power supply and building load [28]. By improving the energy flexibility of appliances, the self-consumption ratio of PV electricity can be increased, which reduces the demand for energy storage batteries and electricity fed back into the grid. Salpakari et al. [29] studied the optimization control of the household appliances powered by PV modules. They found that the cost-optimal control could decrease cost by 13–25% and grid feed-in by 8–88%. Several studies have implemented Model Predictive Control in thermostatically shiftable appliances of buildings equipped with PV panels, including Zhang et al. [30], Zhan et al. [31], and Zong et al. [32]. These studies aimed to reduce electricity costs and increase the consumption of PV electricity. Ghazvini et al. [33] optimized the operation of the electric vehicle, electric water heater, and battery in the building integrated with PV panes. The aim is to minimize the electricity cost compared with the rule-based strategy. Lu et al. [34] optimized the load of the adjustable load to maximize the users' satisfaction and to minimize PV power into the grid. Dual-objective optimization results were used to provide relevant policy recommendations in China. Bahramara et al. [35] proposed a robust optimization method of the postponable appliances connected to roof PV panes, aiming to minimize operation while limiting the ramp rate of grid electricity.

1.2 Novelty and contribution

After reviewing the relevant literature, it is evident that shiftable appliances are widely utilized to enhance building demand flexibility, with the goal of improving the self-consumption ratio of PV

electricity. Nevertheless, the solar utilization efficiency remains limited, as only a fraction of the incident solar radiation is effectively harnessed, with the rest dissipating as heat. In recent years, PV/T technology has emerged as a promising innovation for building integration. This technology not only generates electricity but also recovers heat from the PV modules to produce hot water, significantly increasing solar utilization efficiency [36]. Proposing and investigating the flexible consumption of PV/T energy output can further optimize the solar utilization. However, to the best of our knowledge, scheduling the optimization of household appliances when the building is powered by PV/T modules has been underexplored. Additionally, previous research on the flexible consumption of PV electricity has primarily focused on individual shiftable appliances. In practice, when a building is powered by renewable energy, it is crucial to account for the interplay among various appliances and develop an overarching plan for all types of household devices. The reason is that all appliances must be coordinated to maximize the consumption of renewable electricity while mitigating excessive grid power fluctuations. Therefore, the scheduling optimization of demand flexibility for PV buildings that integrate various types of shiftable appliances is more relevant than addressing individual appliances.

To address these research gaps, this study conducts the scheduling optimization of various shiftable household appliances powered by PV/T modules. The primary objective is to comprehensively investigate the performance and operation strategies of this novel system and compare it with PV powered building. Subsequently, the sensitivity of uncertainty factors on the performance of PV/T powered buildings is analyzed. The novelty and contributions of this study are two aspects: firstly, the optimized building is powered by PV/T modules that not only generate clean electricity but also produce domestic hot water. The presented models and results can serve as a reference for future work on the operation optimization and potential assessment of PV/T technology in buildings. Secondly, in the global optimization process, various types of shiftable appliances are considered, encompassing thermostatically controlled, postponable, continuous, and non-continuous appliances. These appliances are collectively planned to achieve dual objectives: minimizing electricity costs and reducing grid fluctuations. The collaborative approach adopted in this study further enhances the applicability and relevance of the research.

2. System description

2.1. Building energy network

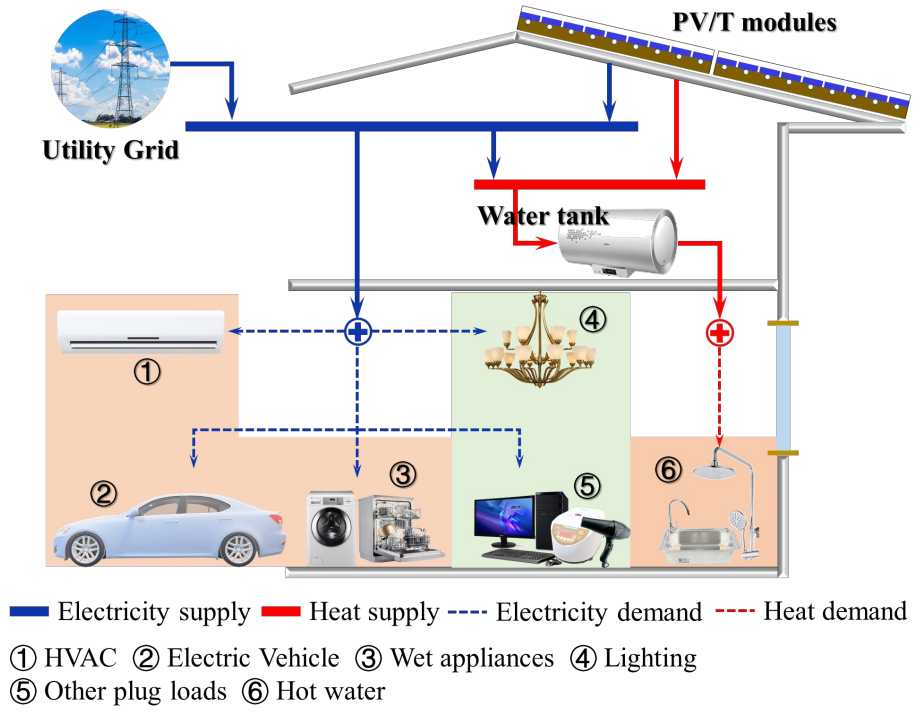

Fig. 1 The system configuration of building powered by PV/T module

The system configuration of the building powered by the PV/T modules is illustrated in Fig. 1. The system components consist of the PV/T modules, the household appliances, the utility grid, and the water tank. The electricity supply is depicted by the solid blue line in the figure, which primarily originates from the utility grid and the PV/T modules. The heat supply is represented by the solid red line. The water tank is heated by the electric water heater (EWH) and the PV/T modules. The dotted lines represent the electricity and heat demand. The water tank provides heat to the building for showering and washing in accordance with the occupant's requirements. The household appliances are classified into two categories: shiftable and non-shiftable appliances. The shiftable appliances can adjust the power consumption and operation time while satisfying the user's needs. In this study, the shiftable appliances considered are the air conditioner (AC), the EWH, the electric vehicle (EV), and the wet appliances. The wet appliances refer to household appliances that involve water or liquid in their operation, such as washing machines, dishwashers, and other similar devices. Generally, the

operation of wet appliances must be continuous. The principles of demand flexibility for these appliances are as follows: (1) the thermal mass of the building can be charged or discharged to modify the AC's power profiles; (2) the heat of the water tank can be stored to shift the EWH's electricity demand; (3) the charging time of the EV can be adjusted within the flexibility window, while ensuring the charging capacity; (4) the use time of the wet appliances can be modified within the flexibility window. Non-shiftable appliances, such as lighting lamps, TVs, and cookers, have relatively constant power consumption and operating periods. Altering their operation may compromise user comfort or not meet the building requirements. Generally, it is encouraged the immediate consumption of electricity generated by PV modules. This is due to the potential harm that PV electricity fed into the grid may cause [37]. Additionally, the high initial investment associated with batteries limits their real-world application in storing PV electricity [38]. Therefore, this study assumes that neither batteries nor PV electricity to the grid is considered. The electricity generated by PV/T modules in the studied system is directly consumed by appliances, and the surplus electricity is dumped.

2.2. Control-oriented model

The objective of this study is to improve the economic and grid stability of the building energy system by controlling the demand profiles of the shiftable appliances. As described in Section 2.1, the controlled shiftable appliances include AC, EWH, EV, and wet appliances, while the non-shiftable loads and the weather data serve as the boundary conditions for the optimization control. In this section, the numerical models of the shiftable appliances and PV/T modules are described in detail.

2.2.1. Thermal dynamics of buildings

The Resistor–capacitor (RC) model is a grey-box model for characterizing the thermal dynamics of the building [39]. This method simplifies the complex energy conservation equations of building into the basic algebraic equations by using the lump capacity and resistance approach. Consequently, it is widely adopted in the optimization and control of buildings. As shown in Fig. 2, the window, wall, and indoor air are modelled by the 1R0C, 3R2C, and 2R1C models, respectively.

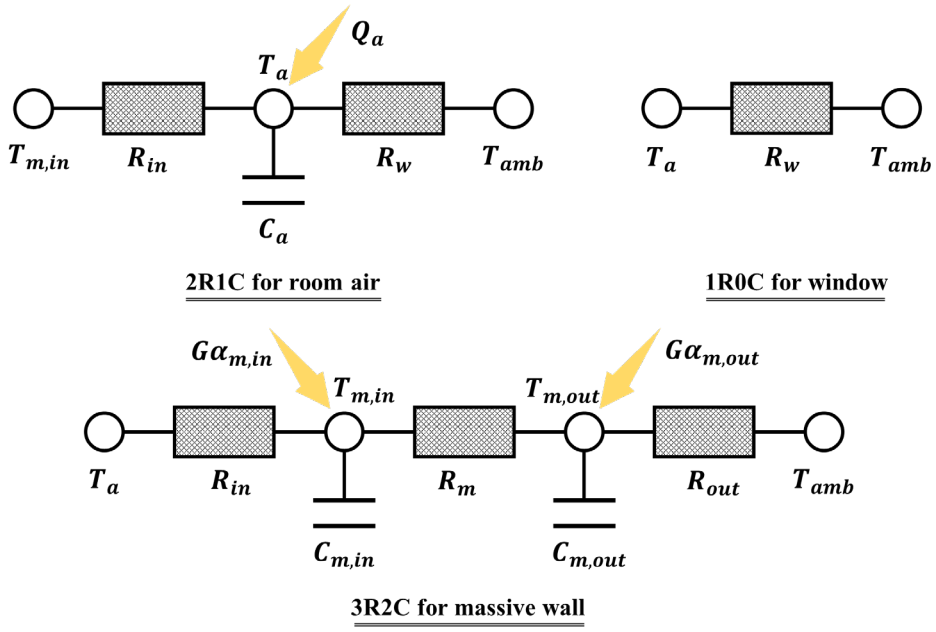

Fig. 2 The used RC models for the studied building

The thermal dynamics can be represented by the three-order state-space equations. They are written as:

$$C_a \frac{\partial T_a}{\partial t} = \frac{T_{w,in} - T_a}{R_{in}} + \frac{T_{amb} - T_a}{R_w} + G\alpha_a + Q_a \quad (1)$$

$$C_{m,in} \frac{\partial T_{m,in}}{\partial t} = \frac{T_a - T_{m,in}}{R_{in}} + \frac{T_{m,out} - T_{m,in}}{R_m} + G\alpha_{m,in} \quad (2)$$

$$C_{m,out} \frac{\partial T_{m,out}}{\partial t} = \frac{T_{m,in} - T_{m,out}}{R_m} + \frac{T_{amb} - T_{out}}{R_{out}} + G\alpha_{m,out} \quad (3)$$

where, T and C respectively are the temperature (°C) and thermal capacity of the nodes (J·K^{-1}). The subscript a, amb, m,in, and m,out respectively represent indoor air, outdoor air, inside and outside surfaces of the massive wall. R_{in} and R_{out} respectively are the thermal resistances (K·W^{-1}) between indoor air and massive wall, between outdoor air and massive wall. R_w and R_m are the thermal resistances of window and massive wall (K·W^{-1}). G and α are respectively the solar radiation (W) and solar absorptivity. Q_a is the heating/cooling capacity generated by the AC (W).

After discretizing the partial differential term, the state-space equations can be reconstructed as:

$$\begin{bmatrix} T_a^{t+1} \\ T_{m,in}^{t+1} \\ T_{m,out}^{t+1} \end{bmatrix} = A_{3\times3} \begin{bmatrix} T_a^t \\ T_{m,in}^t \\ T_{m,out}^t \end{bmatrix} + B_{3\times3} \begin{bmatrix} G^t \\ T_{amb}{}^t \\ Q_a{}^t \end{bmatrix} \quad (4)$$

where, A and B are the coefficient matrix of R and C values, which can be estimated by system

identification [40]. The training data of the system identification is usually obtained from experimental tests or simulation results of professional software.

The capacity of AC is limited by the rate capacity, which can be written as:

$$Q_a^t \le Q_a^{rate} \tag{5}$$

2.2.2. PV/T module

In this study, the linear model proposed by Florschuetz et al. [41] is used to predict the thermal and electrical performance of the PV/T modules. This module is modified from the Hottel-Whillier model [42] considering the energy balance of the heat and electricity. The modified equation is written as:

$$Q_s = A_c F_R\left[\tilde{G}(\tau\alpha) - \widetilde{U_L}(T_{in} - T_a)\right] \tag{6}$$

where, Q_s is the heat output of the PV/T modules (W). A_c and F_R are the surface area (m^2) and heat removal factor of the PV/T modules. τ and α are the transmittance of the glass cover and the absorptivity of absorber plate. T_{in} and T_a are the inlet water temperature and the ambient temperature (°C). $\tilde{G}$, and $\widetilde{U_L}$ are modified solar radiation ($W{\cdot}m^{-2}$) and modified heat loss coefficient ($W{\cdot}m^{-2}{\cdot}K^{-1}$) after deducting the PV output from the energy conservation equation of the absorber plate. They are calculated by [41]:

$$\tilde{G} = G(1 - \frac{\eta_{amb}}{\alpha}) \tag{7}$$

$$\widetilde{U_L} = U_L - G\tau\eta_r\beta_r \tag{8}$$

where, η_{amb} and η_r are the PV efficiency under ambient and reference temperature. β_r is the temperature coefficient of PV cells (K^{-1}). U_L is the heat loss coefficient of the collector ($W{\cdot}m^{-2}{\cdot}K^{-1}$).

In this study, the temperature-difference water circulation is adopted for the PVT modules [43]. As a result, the thermal efficiency of the system remains above 0. The constraint of the heat output of PV/T modules is:

$$Q_s = max\{Q_s, 0\} \tag{9}$$

The electricity output of the PV/T modules is calculated by:

$$P_s = GA_c\tau\eta_0[1 - \beta_r(T_p - T_r)] \tag{10}$$

where, T_p and T_r are the average absorber plate temperature and reference temperature (°C), respectively. η_0 is the PV efficiency under the standard condition. T_p can be calculated by the energy conservation equation of the absorber plate:

$$Q_s + P_s + U_L(T_p - T_a)A_c = G(\tau\alpha)A_c \quad (11)$$

2.2.3. Electric vehicles and wet appliances

The charging of the EV usually occurs outside of office hours and the charging process can be non-continuous. The energy consumption equations are written as:

$$P_v^t = \gamma_v^t \rho_v^t, t \in I_v \quad (12)$$

$$\sum P_v^t \, \Delta t = U_v \quad (13)$$

Where, P_v^t and ρ_v^t are the actual and rate charging power of the electric vehicle (W). I_v is the flexibility time window of the charger electric vehicle. U_v is the daily charging demand (J). γ_v^t is the binary variables, where 1 and 0 represent the on and off of the charger, respectively.

The wet appliances are typically operated when occupants are not at rest. Unlike EV charging, the operation of wet appliances must be continuous. For example, users usually do not interrupt the washing machine until the washing cycle is completed. The equations are written as:

$$P_e^t = \gamma_e^t \rho_e^t \quad (14)$$

$$\sum_{t=e}^{t=d-(N-1)} \gamma_e^t \gamma_e^{t+1} \cdots \gamma_e^{t+N-1} = 1 \quad (15)$$

Where, P_e^t and ρ_e^t are the actual and rate power of the wet appliance (W). γ_e^t represents the on/ off of the machines. *e* and *d* respectively represent the beginning and end of the flexibility window for wet appliances. *N* is the number of the operation time steps of wet appliances.

2.2.4. Electric water heater

The water tank primarily plays the role of heat storage and provides heat to the building. The energy balance equation involves the heat gain, the heat release, and the heat loss to the environment. It is written as:

$$S_t^t - S_t^{t-1} = (P_t^{t-1}\eta_t - Q_t^{t-1} - Q_{loss}^{t-1})\Delta t \quad (16)$$

$$S_t = \rho C V (T - T_0) \quad (17)$$

$$Q_{loss}^t = U_{loss}^t A (T^t - T_a^t) \quad (18)$$

where, S_w represents the heat stored in the tank (J). ρ, C, and V represent water density (kg/m^3), specific heat capacity (J·kg^{-1}·K^{-1}), and tank volume (m^3), respectively. T_0 is the initial temperature of water tank (℃). Q_{loss} is the heat loss of water tank (W).U_{loss} are the heat transfer coefficients of

water tank ($W \cdot m^{-2} \cdot K^{-1}$). A is the surface area of water tank (m^2). η_t is the efficiency of the electrical heater.

During the use period, the water temperature should be higher than the target temperature of the user's water. In addition, the water temperature is always lower than the evaporation temperature. Thus, the constraints are written as:

$$T^t \geq T_{tar}, t \in I_t \tag{19}$$

$$T^t \leq T_{eva} \tag{20}$$

where, T_{tar} and T_{eva} are respectively the target temperature and the evaporation temperature (℃). I_t is the hot water using time.

The power of electrical water heater is limited by its rate power. It is written as:

$$P_t^t \leq P_t^{rate} \tag{21}$$

2.3 Case study

In this study, a single-room civil building located in Shenzhen, China was selected as the subject of investigation. The size of the room is 4m (west-east)×3m (north-south) ×2.8m (high). A clear window with the size of 3m (width)×1 m (high) is installed on the south façade of the studied building. The construction of the building envelopes is the common brick with the thickness of 28 cm. Obtaining the R and C values of the RC model with real data is a recognized means to enhance its reliability. Unfortunately, due to the limitations of our research conditions, access to realistic building data was unattainable. In this study, the annual temperature variation of the case building was simulated using the TRNSYS software and the simulation results were used to estimate the R and C values. During the simulation process, solar radiation and ambient temperature inputs in Equation (4) were sourced from local typical meteorological year weather data, while AC heating/cooling power was generated using random numbers. Subsequently, 70% of the simulated temperature results were imported into the system identification toolbox of Matlab software to determine the R and C values. The remaining 30% of the data were then used to validate the obtained RC model. The validation results show that the Cv(RMSE) is 17% and the MBE is 0.43%, satisfying the accuracy requirement for building simulation [44]. Shenzhen (22.62N, 114.07E) is a cooling-dominant area in China and falls within the subtropical region. Thus, there is only the cooling demand throughout the year.

According to the GB50736-2012 in China [45], the setting temperature for cooling is 24℃. The electrical consumption of the air-conditioners is calculated by dividing the cooling load by the performance coefficient of the air conditioner. According to the GB 19576-2019 in China [46], the performance coefficient of the air conditioner used in this study was assumed to be 2.90. Two PV/T modules, each with an irradiated area of 2 m^2, were installed on the roof of the building at the 30° inclination. The studied wet appliances include the washing machine (WM) and the dishwasher (DW). Considering the actual user customs, the charging of the EV only occurs during the parking time. The WM is assumed to work during the daytime and the DW works after the diner. The detailed parameter for planning is listed in Table 1 and the time step for simulation is 20 minutes.

Table 1 Parameters of the studied system

Parameter	Value
PV/T modules	
Heat removal factor	0.81
Heat loss coefficient	8 $W \cdot m^{-2} \cdot K^{-1}$
PV efficiency under standard condition	17%
Temperature coefficient of PV cell	0.0045 K^{-1}
Transmittance of the glass cover	0.85
Absorptivity of absorber plate	0.9
Air conditioner	
Rate power	3000W
COP	2.9
Setting temperature	24℃
Water tank	
Volume	0.2 m^3
Power limit of electrical heater	4000 W
Heat loss coefficient	0.5 $W \cdot m^{-2} \cdot K^{-1}$
Efficiency of electrical heater	0.95
Electric vehicle	
Charging power	1000 W
Daily charging capacity	7 kWh
Flexibility window	0:00~8:00, 12:00~14:00, 18:00~24:00
Washing machine	

Rate power	500 W
Daily work time	60 min
Flexibility window	8:00~18:00
Dishwasher	
Rate power	1200 W
Daily work time	40 min
Flexibility window	18:00~23:00

The electricity consumption of the non-shiftable appliances, except for the lamps, is assumed according to the occupant habits, and the corresponding results are presented in Fig. 3. The lighting consumption of the studied building is predicted by EnergyPlus software, and the weather data of the Typical Meteorological Year of Shenzhen was used as the boundary conditions. The simulation parameters used in the software are listed in Table 2. It was assumed that there were three people living in the studied room. Following the GB 50015-2019 [47], the daily demand for hot water is 300 L, and the schedule of using water is shown in Fig. 3. The heating load required to meet the hot water demand is determined by multiplying the water's heat capacity and the temperature difference between the target temperature (45 ℃) and the groundwater temperature in Shenzhen, which is obtained using the EnergyPlus software. The time-of-use tariff in Shenzhen is shown in Fig. 4. The valley-price period is 00:00~8:00 and the high-price period is 8:00~10:00 and 12:00~14:00 while other time is flat-price period. The corresponding prices for the high, flat, and valley periods are 1.12, 0.6628, and 0.2572 yuan/kWh, respectively.

Table 2 Parameter settings in EnergyPlus software

Parameter	Value
Reference point for lighting	2 m(X), 1.5 m(Y), 0.8 m(Z)
Artificial lighting density	9 W/m^2
Occupy time	8:00-22:00
Illuminance setting value	500 lux

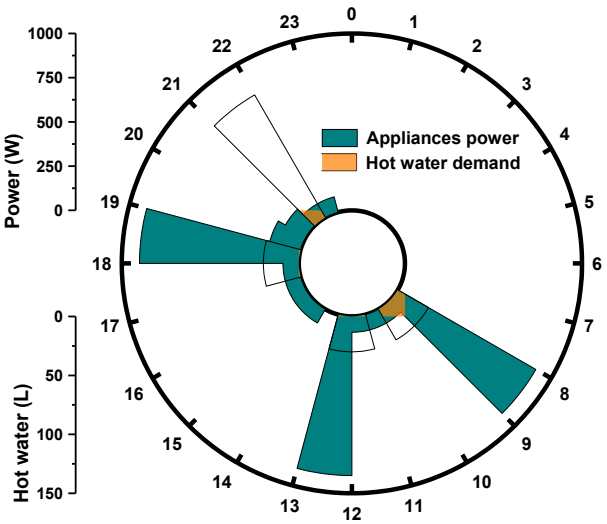

Fig. 3 The schedule of the household electricity appliances and hot water demand

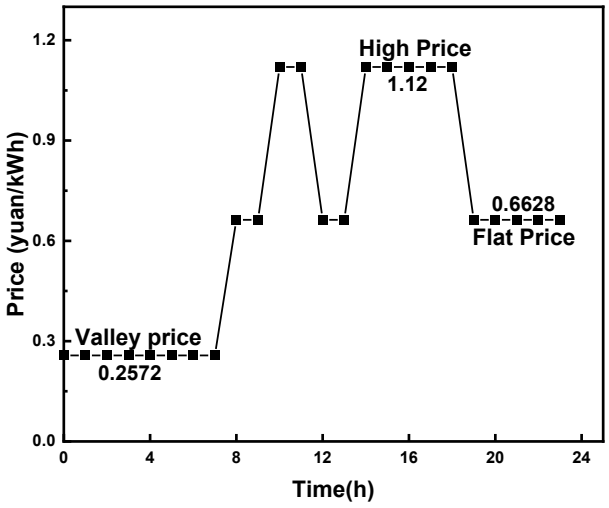

Fig. 4 The dynamic retail price of the electricity in Shenzhen [48]

3. Demand flexibility strategy

As described in 2.1 Section, the work schedule of the shiftable appliances can be adjusted when the constraint is satisfied. Thus, properly planning the work schedules of the shiftable appliances can help achieve peak shaving and valley filling, which is crucial in improving the overall performance of the building energy system, including the decrease of operation cost and grid stability. In this section, an Optimization-based strategy was proposed for controlling the running of the studied building system. The conventional demand flexibility strategy based on the price signal is used for comparison.

3.1. Benchmark strategy

In this study, the Price-based demand flexibility strategy is used as the benchmark for comparison [8]. This strategy aims to increase the building energy consumption during low electricity price periods and decrease it during high price periods. For the air conditioner, the cooling set temperature is increased by 2℃ when the hourly electricity price is at its highest. When the electricity price is lowest, the set temperature is decreased by 2℃. Otherwise, the set temperature is the standard setting. The electrical water heater for the water tank is used to keep the water temperature above the target temperature. For the other shiftable appliances, they are programmed to work during the lowest tariff period within their flexibility window. Based on the time-of-use tariff of Shenzhen, the washing machine and dishwasher are scheduled to work at 12:00~13:00 and 19:00~19:40, respectively. The electric vehicle is charged during the time period of 0:00 to 7:00.

3.2. Optimization strategy

In this study, the schedule planning of the household appliances is formulated as an optimization problem. The purpose of optimization is to search the values of decision variables that minimize the value of the objective function while satisfying all restrictions. The decision variables include the air-conditioning temperature, and the power consumption of the electrical water heater, electrical vehicle, and wet appliances. The basic restrictions are established through the Equations (1-21). For the studied building energy system, the goal of optimization is to reduce the operation cost and fluctuation of the grid power. The objective function for optimization is written as:

$$min\ obj = \alpha P_g^{max} + \sum_{t=1}^{N} P_g^t C_{ele}^t \tag{22}$$

where, C_{ele}^t and P_g^t are respectively the tariff and grid power consumption during the operation process. P_g^{max} is the maximum value of the grid power during the optimization horizon and α is the weight factor. *N* is the optimization horizon.

As described in 2.1 Section, PV power is used directly by appliances, and surplus power is dumped. The grid power consumption is calculated by:

$$P_g^t = max\ \{P_a^t + P_v^t + P_t^t + P_e^t + P_o^t - P_s^t\ ,0\} \tag{23}$$

where, P_o^t is the electricity power of the non-shiftable appliances.

The maximum value of the grid power is calculated by:

$$P_g^{max} = max\ \{P_g^1, P_g^2, \cdots P_g^N\} \tag{24}$$

In this study, the weight factor is defined as:

$$\alpha = \frac{C_b}{P_b^{max}} \tag{25}$$

where, C_b and P_b^{max} are the total electricity cost and the maximum value of the grid power when the operation strategy is the benchmark strategy during the current optimization horizon.

The nonlinear constraints in the optimization problem often significantly increase the complexity of the solution and may lead to solution failure. Before conducting the optimization, the nonlinear equations Equations (15) and (24) were transformed into the linear constraints by introducing intermediate variables [49]. After that, the present optimization problem is converted into the Mixed Integer Linear Program (MILP), which can be solved by mathematical programming methods to obtain the global optimal solution. The flowchart of the optimization-based strategy is shown in Fig. 5. The optimization is performed over the sequential 24-h horizon (72 timesteps). The end state of the temperature of the indoor air, wall, and water tank was reinput as the initial value of the next optimization horizon. The optimization solver is the IBM CPLEX Optimizer 12.9.

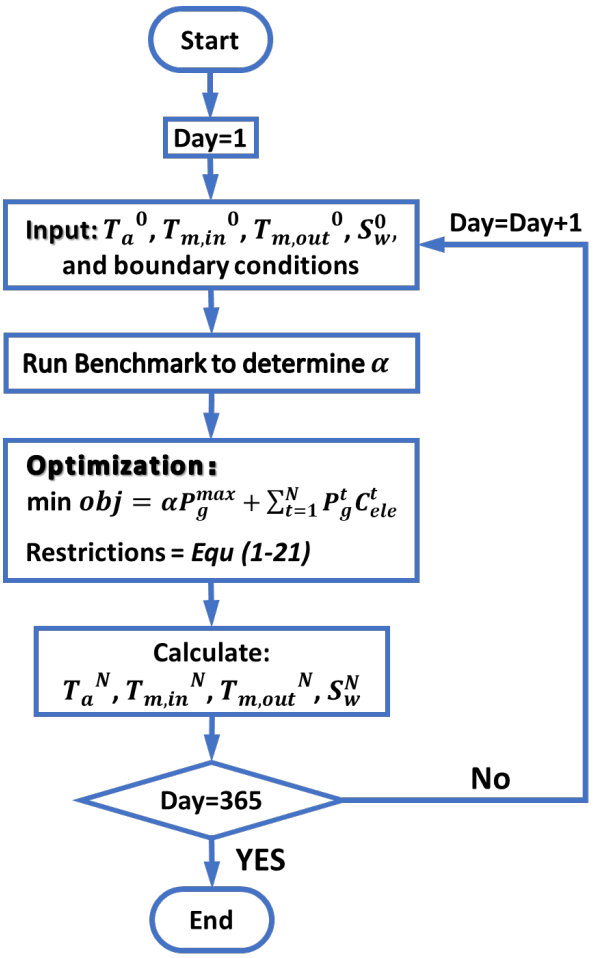

Fig. 5 The operation flowchart of the optimization-based strategy during the whole year

4. Results and discussion

4.1. Performance evaluation of demand flexibility strategy

This section gives a detailed analysis of the daily energy flow and annual performance of the studied system under both the benchmark and optimization strategies. The energy flow analysis includes the energy consumption of all investigated appliances and the output of the PV/T modules. Furthermore, the annual performances are evaluated by the electricity cost, maximum grid power, and solar energy utilization. The calculation methods of daily electricity cost and maximum grid power have been described in 3.2 section. The solar energy utilizations of PV/T or PV modules are calculated by:

$$E_e = \sum_{t=1}^{N} max\left\{P_s^t, P_a^t + P_v^t + P_t^t + P_e^t + P_o^t\right\} \Delta t \quad (26)$$

$$E_t = \sum_{t=1}^{N} Q_s \, \Delta t \quad (27)$$

where, E_e and E_t are the daily solar energy utilizations of electricity and heat, respectively.

4.1.1. Daily energy flow analysis

The power consumption of the air conditioner and the corresponding room temperature under the two demand flexibility strategies are shown in Fig. 6. As the actual AC power is always lower than its rated power, the room temperature is equal to the cooling set point temperature when the AC is running. Under the benchmark strategy, the room temperature is 26℃, 24℃, and 22℃ during the high, flat, and valley tariff periods, respectively. Under the optimization strategy, the room temperature is 26℃ during 0:00-2:00, 12:40-13:20, and 14:20-24:00, while it is 22℃ during 7:20-8:20. In other periods, the room temperature ranges from 22℃ to 26℃. It can be observed that the room temperature is lower at night and higher in the afternoon. The building's thermal mass stores the cooling energy when the tariff is low and releases it when the tariff is high. There is no AC power consumption between 8:00-10:00 under the optimization strategy due to the cold storage. Additionally, the AC power consumption under the optimization strategy is much higher than that under the benchmark strategy between 10:00-12:20. The reason is that the optimization strategy intends to consume the surplus PV electricity.

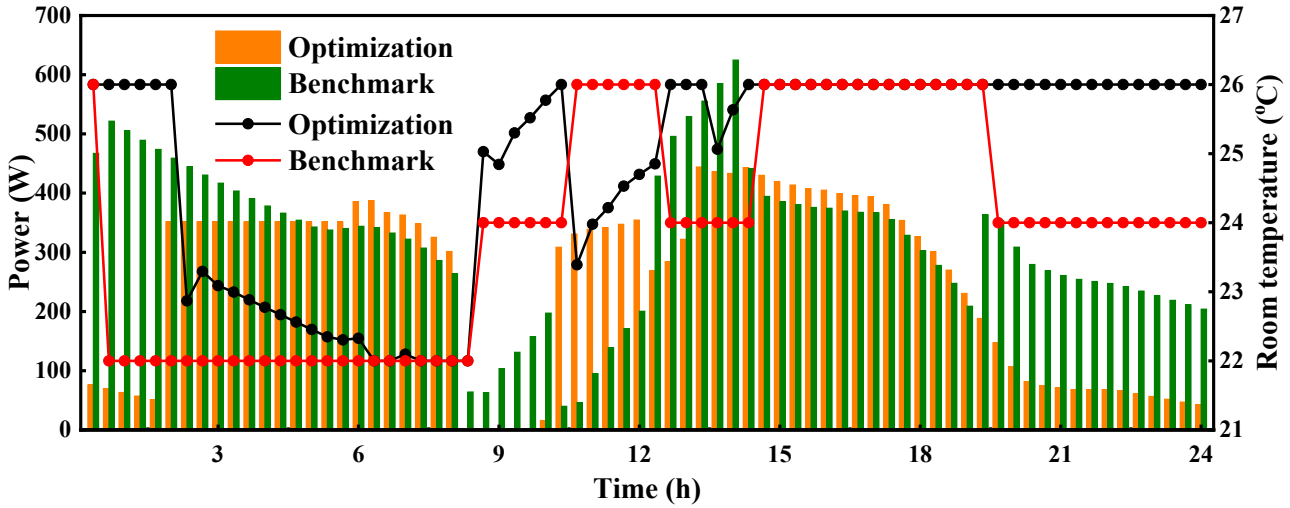

Fig. 6 The power consumption of the AC and room temperature during one day

The power consumption of the EWH and water temperature under the two demand flexibility strategies are shown in Fig. 7. From 9:00 to 24:00, the water temperature under the two demand strategies is the same because the heat demand is entirely provided by the PV/T modules. The

maximum temperature is 68.9℃ from 16:20 to 17:20. Between 9:20 and 16:20, the heat gain of the water tank is completely supplied by the PV/T modules. The biggest difference between the studied two strategies is the EWH power. Under the benchmark strategy, the maximum power is above 2000 W, which occurs at the initial moment aiming to raise the water temperature to above 45℃. Subsequently, the EWH provides continuous small power to offset heat loss from the tank. In contrast, the optimization strategy divides the EWH power into multiple time periods to stagger the electricity peaks while raising the water temperature to the set point.

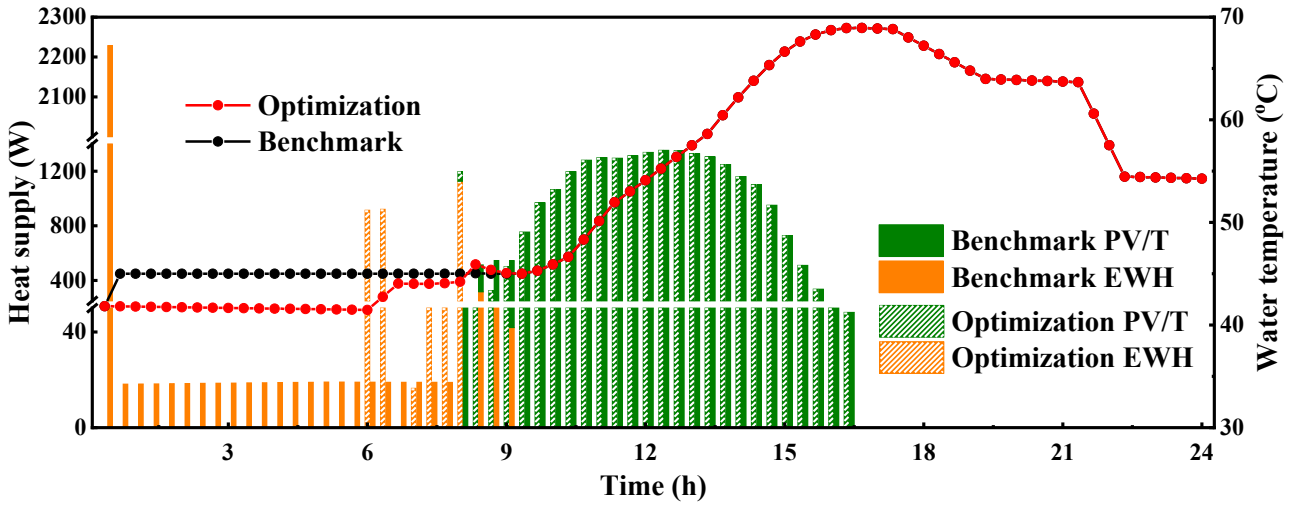

Fig. 7 The water temperature and the heat supply of the EHW and PV/T modules during one day

The power consumptions of the postponable appliances are shown in Fig. 8. Under the benchmark strategy, all appliances are scheduled to operate during pre-determined time periods. Under the optimization strategy, the operation time of the appliances is shifted to minimize the optimization objective. For instance, the EV charging is scheduled between 0:00-6:00 and 6:40-7:40. The vacant period between 6:00-6:40 is utilized to stagger with other electrical appliances. The WM works between 9:00-10:00, which is also the period with the lowest tariff in the flexibility window of the WM. The DW operation time under the optimization strategy is delayed compared to that under the benchmark strategy, with the objective of staggering with other electrical appliances.

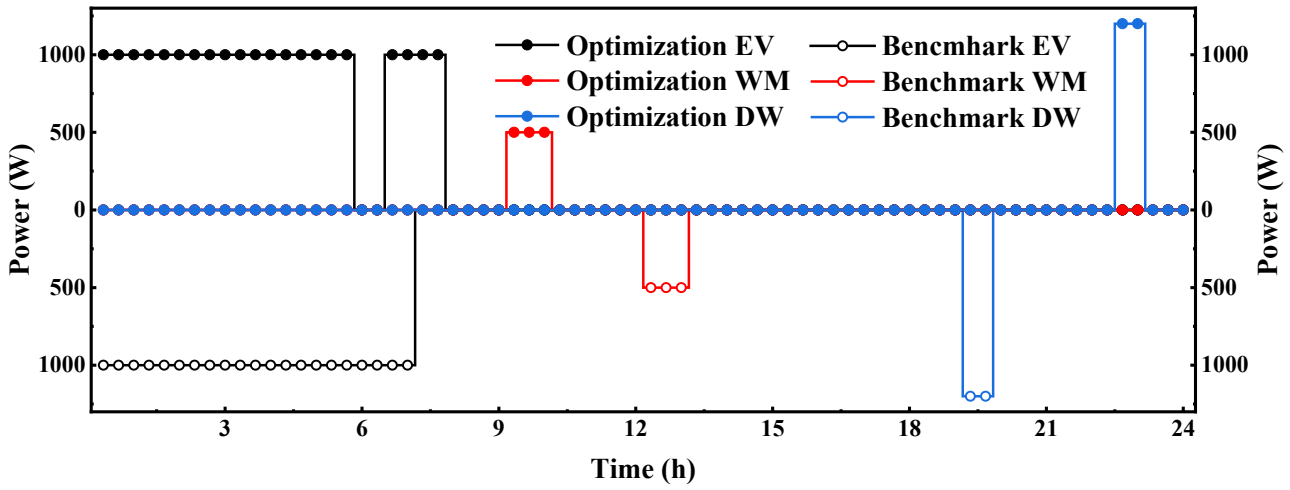

Fig. 8 The power consumption of the postponable appliances during one day

The grid electricity consumption of the studied system and the electricity generated by the PV/T modules is shown in Fig .9. The maximum grid power of the benchmark strategy is 3813W at 0:20, which is primarily used for EWH to heat water from the initial temperature to the target temperature. In contrast, the optimization strategy shows a relatively gentle change in grid power, with a maximum power of 1351W at 8:00. Between 9:20 and 12:00, the total power consumption of the benchmark strategy is lower than the power generated by the PV/T modules. Thus, the grid power is zero and the surplus PV/T electrical power is dumped as shown in the shaded part in Fig. 9. The total dumped power is 0.53 kWh in the analyzed day. The optimization strategy shifts the power consumption of the appliances to this period, allowing for the consumption of the full renewable energy and reducing the electricity cost. After summing, the daily electricity consumption from the utility grid for the benchmark and optimization strategies are 18.4 kWh and 16.2 kWh, respectively. The daily costs for the benchmark and optimization strategies are 8.76 yuan and 7.58 yuan, respectively.

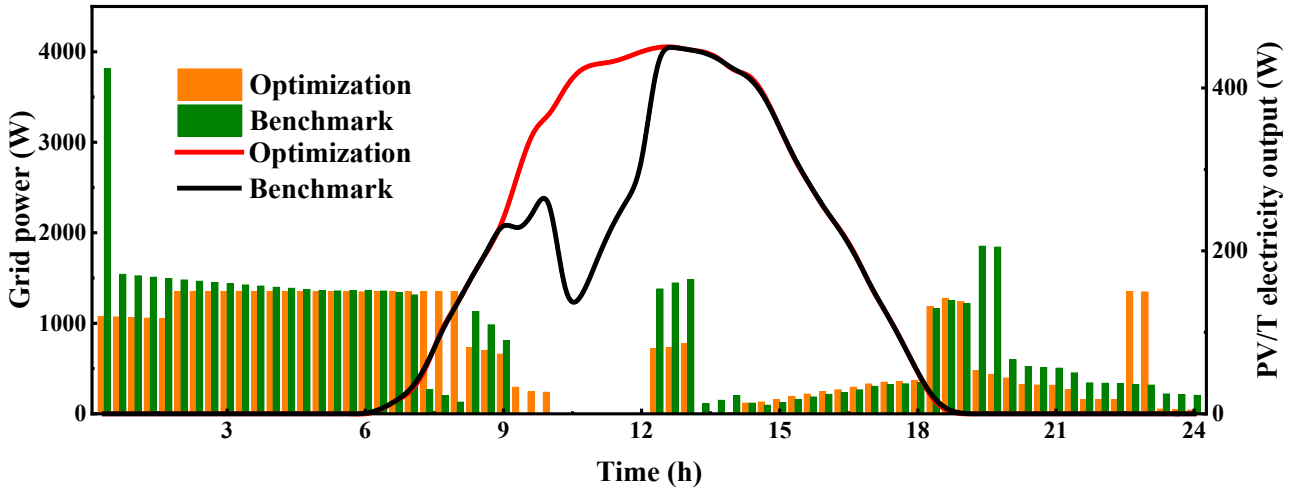

Fig. 9 The grid power consumption and the PV/T electricity output during one day

4.1.2. Annual performance evaluation

The daily electricity cost during the whole year is shown in Fig. 10. It is evident that the optimization strategy consistently yields lower daily costs than the benchmark strategy. The changing tread of the electricity cost is high in winter and low in summer. The reason is that the energy consumption of water heating in winter is much higher due to the low temperature of groundwater. However, the optimization strategy utilizes more PV electricity for water heating, thereby increasing the renewable energy utilization rate and reducing electricity costs significantly. In summer, the PV/T modules can meet most of the water heating needs, which results in PV electricity being consumed primarily by the AC system. As shown in Fig. 10, since the building's insulation is worse than that of the water tank, the reduction in electricity costs in winter is higher than in summer. After summing, the annual electricity costs under the benchmark and optimization strategies are 2770 yuan and 3412 yuan, which means that the electricity cost is reduced by around 19%. The daily maximum power of the studied system is shown in Fig. 11. Similar to the trend in electricity cost, the maximum power consumption varies greatly with the seasons, with higher maximum power in winter and lower in summer. The maximum power of the optimization strategy is consistently lower than that of the benchmark strategy. The maximum power of the optimization strategy ranges from 1290 W to 2160 W while the maximum power of the benchmark strategy is almost between 1500 W and 3800 W. Therefore, over the course of one year, the optimization strategy is more economical and grid-friendly than the benchmark strategy.

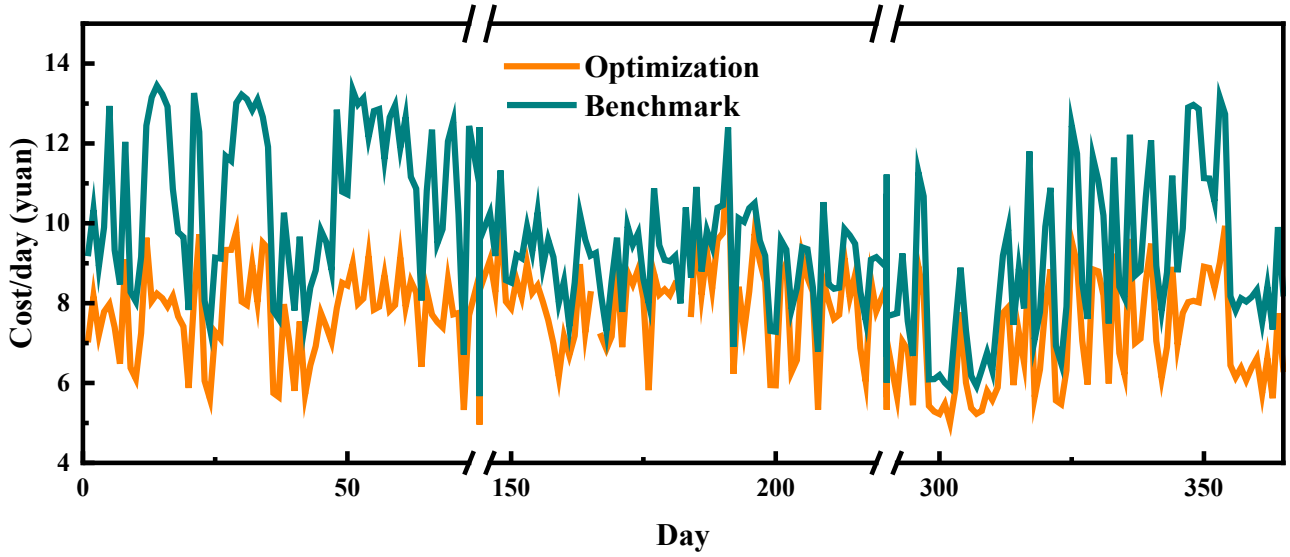

Fig. 10 The daily electricity cost of the demand flexibility strategies during the whole year

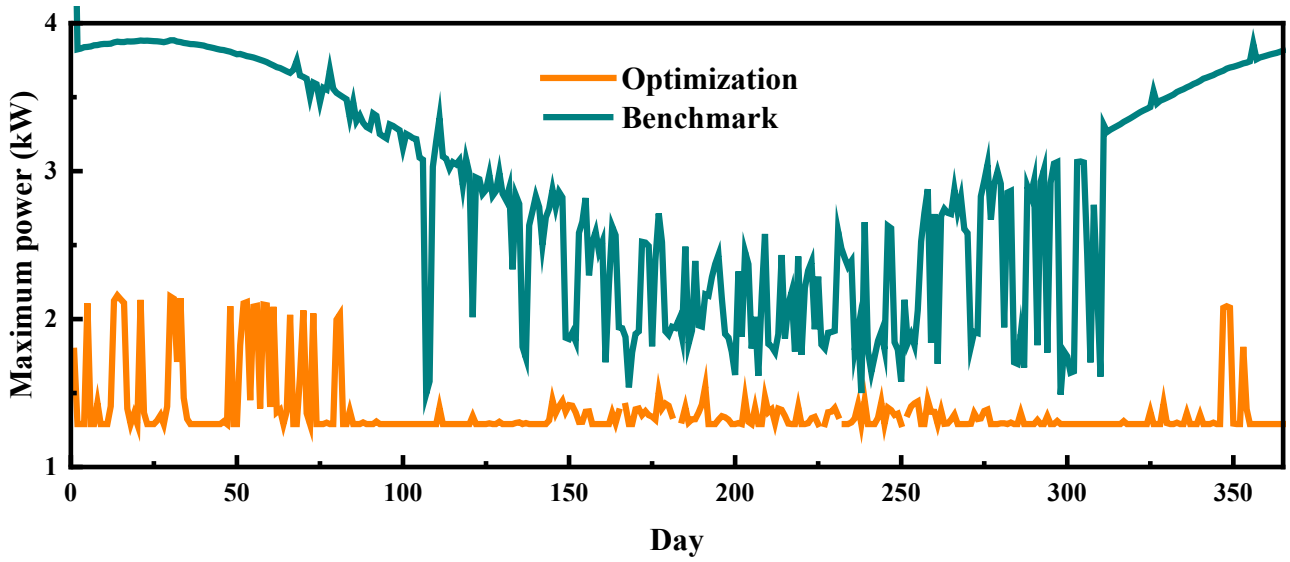

Fig. 11 The daily maximum grid power of the demand flexibility strategies during the whole year

The daily utilization of PV electricity over the entire year is presented in Fig. 12. The utilization of PV electricity is consistently higher for the optimization strategy compared to the benchmark strategy. Because there is no cooling load during the winter daytime, the surplus PV electricity of the benchmark strategy is dumped. It can be found that the PV output of the benchmark strategy is much lower. For the optimization strategy, the surplus PV output is used to heat water and the PV output is high during the whole year. After summing, the utilized electricity output of the PV/T modules is 797 kWh for the optimization strategy and 597 kWh for the benchmark strategy. Fig. 13 illustrates the

daily utilized heat output of the PV/T modules over the whole year. It can be observed that the heat output of the optimization strategy is slightly lower than that of the benchmark strategy. The reason is that the optimization strategy often raises the water temperature in the valley price. The thermal efficiency of the PV/T modules is decreased when the inlet water temperature is high. Overall, the utilized heat output of the PV/T modules is 1220 kWh for the optimization strategy and 1302 kWh for the benchmark strategy.

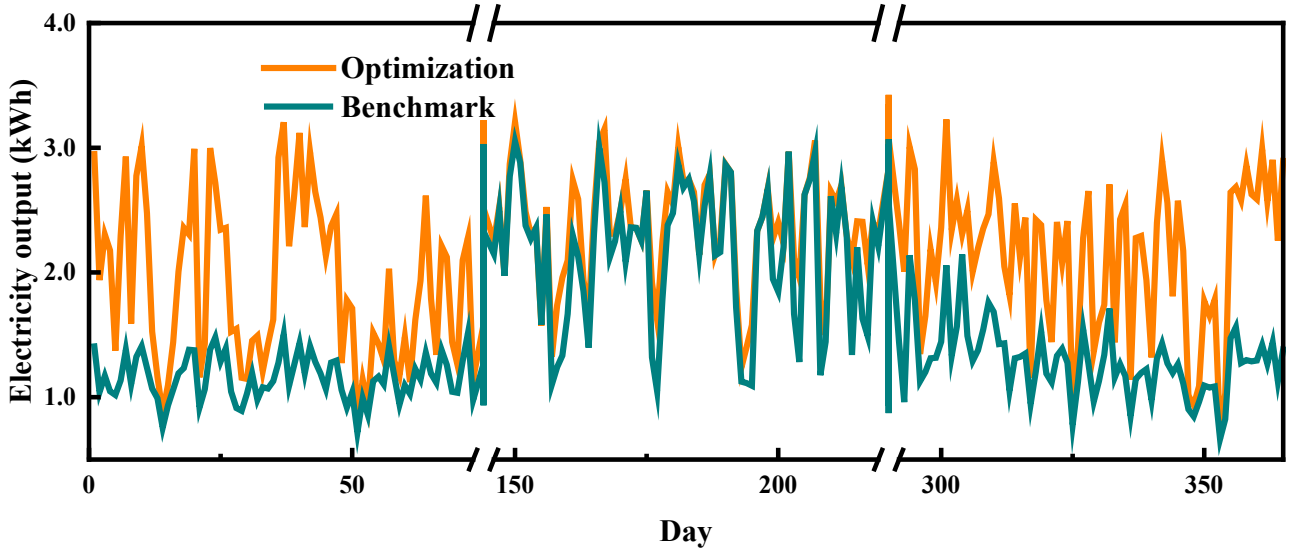

Fig. 12 The daily electricity output of the PV/T modules during the whole year

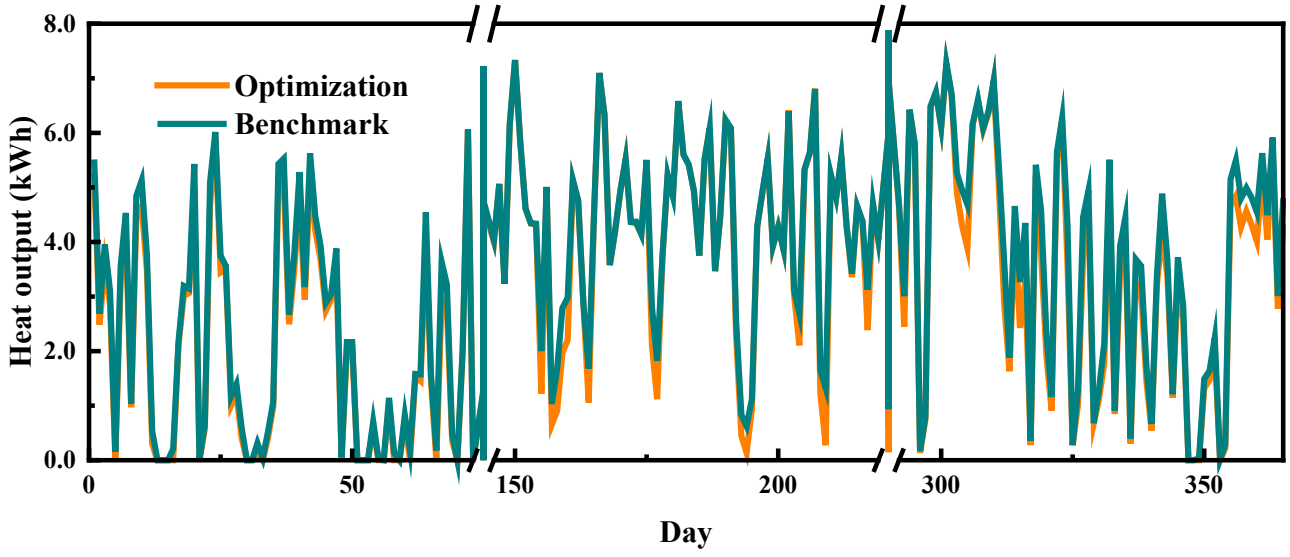

Fig. 13 The daily heat output of the PV/T modules during the whole year

4.2. Comparison between the PV/T module and PV module

The previous section demonstrated that the proposed optimization strategy can not only reduce the electricity cost but also smooth the grid power. This section compares the annual operation results of a building powered by PV/T modules and PV modules under the optimization strategy. Fig. 14 shows the annual building electricity cost and the utilized solar energy of the two systems. The electricity output of the PV/T modules is lower than that of the PV modules due to reduced radiation incident on the PV cells caused by the glass cover of the PV/T modules. However, the PV/T modules can supply a significant amount of heat. After summing, the solar energy utilization of the PV/T modules is approximately double that of the PV modules. The annual electricity costs for the PV/T modules and PV modules are 2770 yuan and 3046 yuan, respectively. The statistical results of the daily maximum grid power during the whole year are shown in Fig .15. The daily maximum power for the building powered by PV/T modules varies from 1290 W to 2490 W, while the values for the building powered by PV modules range from 1290 W to 2160 W. The statistical results of the annual maximum grid power reveal that the maximum power of the PV/T modules is mostly below 1400 W, accounting for 89%. In contrast to this, the daily maximum power below 1400W accounts for only 44% for the building powered by the PV modules. Therefore, it can be concluded that the building powered by the PV/T modules has better grid friendliness.

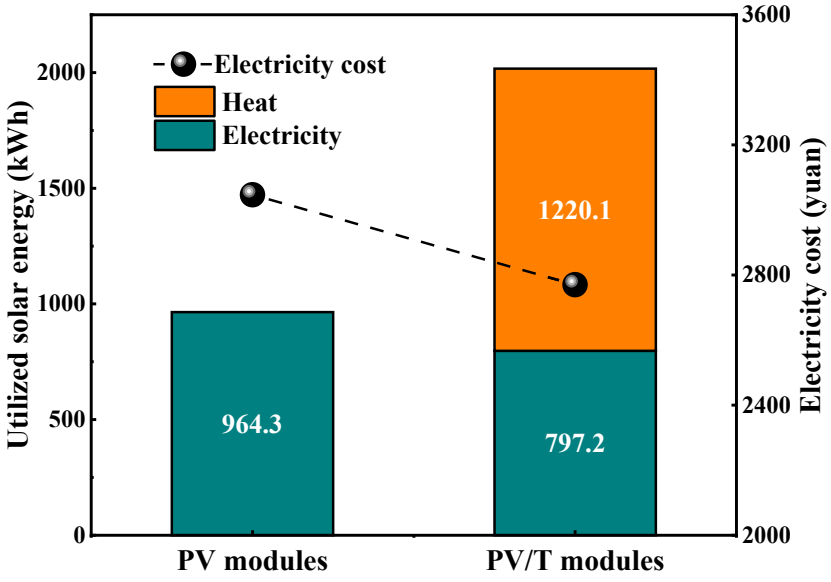

Fig. 14 The electricity cost and utilized solar energy of buildings powered by PV and PV/T modules

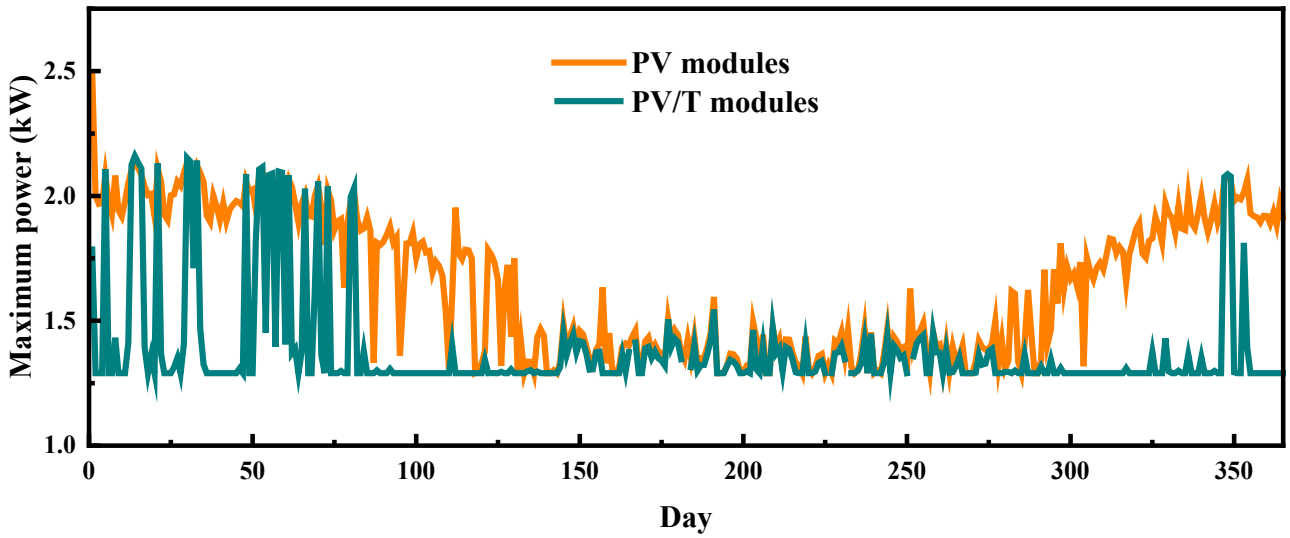

Fig. 15 The daily maximum grid power of buildings powered by PV and PV/T modules

4.3. Sensitivity analysis of uncertainty factor

The optimization strategy relies on the accurate prediction of boundary conditions, such as weather data, indoor heat sources, and inflexible loads. In this section, the effect of uncertainty of boundary conditions on the optimization results is analyzed. The analyzed weather data are the solar radiation and ambient temperature, where the irradiation on the building envelope and PV/T module were analyzed separately. The indoor heat source including the people activities, air infiltration, and indoor ventilation, et al, only affect the AC load. In this study, the uncertainty of the indoor heat source is represented by the forecast error of the AC power. The relative error for all boundary conditions is assumed to be within 10%. To assess the impact of the uncertainty of boundary conditions, all appliances run 1000 times with the optimized results in 4.1.1 section while the uncertainty factor being analyzed is randomly generated for each run. The statistics of the electricity cost and maximum grid power are shown in Fig. 16-17. It can be found that the both electricity cost and maximum power tend to be worse when the boundary conditions are different from the predicted values. Among all boundary conditions, the ambient temperature has the highest impact on the optimization results, followed by irradiation on the PV/T modules. The reason is that the ambient temperature affects both cooling load, water-heating load, and PV/T output. The electricity cost with the uncertain ambient temperature is between 7.5 yuan and 9.0 yuan, while the maximum power is between 1535 W and 1800 W. The average deviations of the electricity cost and maximum power are 8.4% and 23.3%,

respectively. When the irradiation on the PV/T module is uncertain, the electricity cost and maximum grid power are 7.6~8.0 yuan and 1350~1420 W, respectively. The average deviations are 1.9% and 1.5%, respectively. Thus, ensuring accurate ambient temperature prediction is critical for day-ahead scheduling optimization, followed by accurate prediction of irradiation on the PV/T module, the forecast accuracy of which can be reduced by shading from trees or other obstructions.

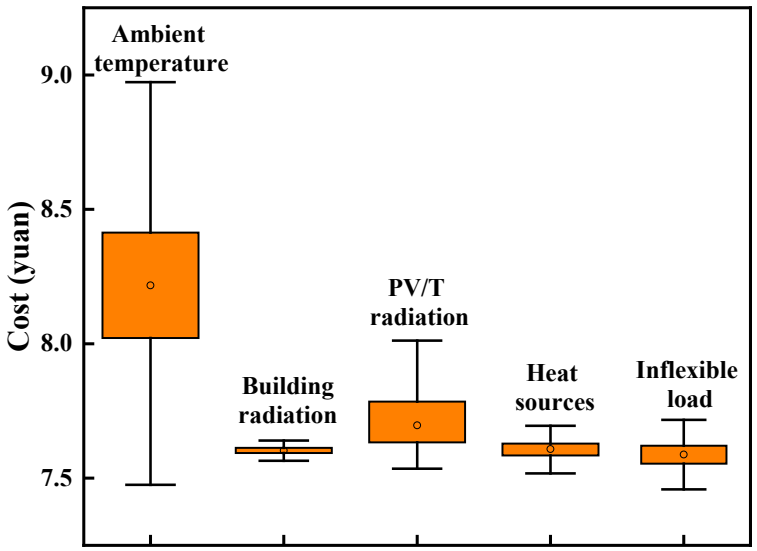

Fig. 16 The effect of the uncertainty factor on the electricity cost

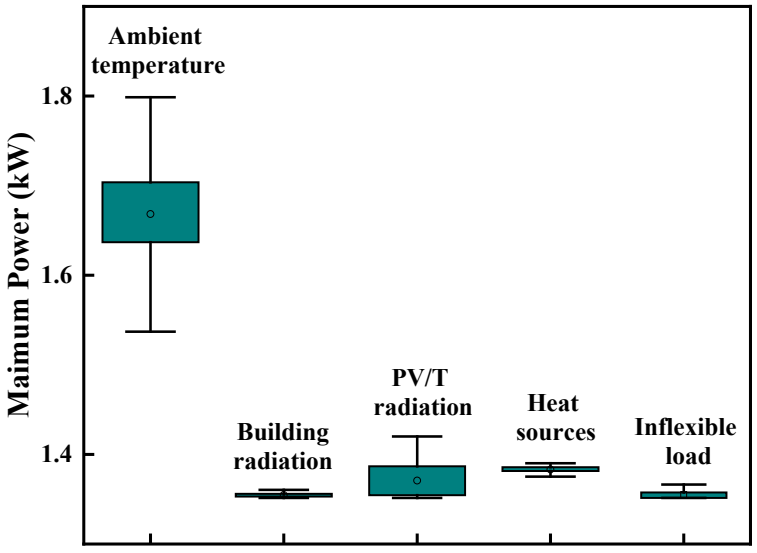

Fig. 17 The effect of the uncertainty factor on the maximum grid power

5. Conclusion

In this study, the day-head operation schedule of household shiftable appliances in the PV/T

powered building was investigated for demand flexibility. A Mixed Integer Linear Program model was developed to optimize the operation schedule, which is referred to as the optimization strategy. The price-based strategy, called the benchmark strategy, was used for comparison. A single-room building with the PV/T modules and various appliances in Shenzhen was analyzed as a case study. Firstly, the daily energy flow and the annual performance of the optimization and benchmark strategies were evaluated. Then, the annual performances of the buildings powered by the PV/T and PV modules were compared in terms of the electricity cost, solar energy utilization, and effect on the grid. Finally, the effect of uncertainty in the boundary conditions on the optimization results was discussed. The results are summarized as follows:

(1) The optimization-based strategy can coordinate the operation of all appliances to increase the consumption of renewable energy. Compared to the benchmark strategy, the optimization strategy could reduce the annual electricity cost by 23% and smooth the daily grid power fluctuations. Furthermore, the optimization strategy increases the electricity output of the PV/T modules while decreasing the heat output. Therefore, it is crucial to reasonably design the heat and electricity output ratio of the PV/T modules when using the optimization strategy.

(2) The utilization of solar energy with the optimization demand flexibility strategy in PV/T modules is twice as high as that in PV modules. Compared to a building powered by PV modules, a building powered by PV/T modules could reduce the electricity cost by 10% and significantly smooth the grid power fluctuation.

(3) The forecast error of boundary conditions, such as weather data, indoor heat sources, and non-shiftable loads, had a negative effect on the electricity cost and grid power fluctuations. Among them, the greatest impact was caused by the ambient temperature and the irradiation on the PV/T modules surface. Therefore, it is recommended to focus on improving the forecast accuracy of ambient temperature and avoiding shading on the PV/T surface for operation optimization of the building powered by the PV/T modules.

6. Acknowledgement

This work was supported by the research funding of the Joint Postdoc Scheme with Non-local Institutions of The Hong Kong Polytechnic University.

Reference

[1] Agency IE. Buildings. 2023.

[2] Cabeza LF, Ürge-Vorsatz D, Palacios A, Ürge D, Serrano S, Barreneche C. Trends in penetration and ownership of household appliances. Renewable and Sustainable Energy Reviews. 2018;82:4044-59.

[3] Forero-Quintero J-F, Villafáfila-Robles R, Barja-Martinez S, Munné-Collado I, Olivella-Rosell P, Montesinos-Miracle D. Profitability analysis on demand-side flexibility: A review. Renewable and Sustainable Energy Reviews. 2022;169.

[4] Xiao Z, Gang W, Yuan J, Chen Z, Li J, Wang X, et al. Impacts of data preprocessing and selection on energy consumption prediction model of HVAC systems based on deep learning. Energy and Buildings. 2022;258.

[5] Chen Y, Xu P, Gu J, Schmidt F, Li W. Measures to improve energy demand flexibility in buildings for demand response (DR): A review. Energy and Buildings. 2018;177:125-39.

[6] Aghniaey S, Lawrence TM. The impact of increased cooling setpoint temperature during demand response events on occupant thermal comfort in commercial buildings: A review. Energy and Buildings. 2018;173:19-27.

[7] Le Dréau J, Heiselberg P. Energy flexibility of residential buildings using short term heat storage in the thermal mass. Energy. 2016;111:991-1002.

[8] Foteinaki K, Li R, Péan T, Rode C, Salom J. Evaluation of energy flexibility of low-energy residential buildings connected to district heating. Energy and Buildings. 2020;213.

[9] Chen Y, Xu P, Chen Z, Wang H, Sha H, Ji Y, et al. Experimental investigation of demand response potential of buildings: Combined passive thermal mass and active storage. Applied Energy. 2020;280.

[10] Liu M, Heiselberg P. Energy flexibility of a nearly zero-energy building with weather predictive control on a convective building energy system and evaluated with different metrics. Applied Energy. 2019;233-234:764-75.

[11] Troitzsch S, Sreepathi BK, Huynh TP, Moine A, Hanif S, Fonseca J, et al. Optimal electric-distribution-grid planning considering the demand-side flexibility of thermal building systems for a test case in Singapore. Applied Energy. 2020;273.

[12] Fan M, Song S. Energy flexibility of space-heating or cooling in Spain based on Developed Wildebeest Herd Optimization algorithm. Energy Reports. 2022;8:10913-22.

[13] Ding Y, Bai Y, Tian Z, Wang Q, Su H. Coordinated optimization of robustness and flexibility of building heating systems for demand response control considering prediction uncertainty. Applied Thermal Engineering. 2023;223.

[14] Kapsalis V, Hadellis L. Optimal operation scheduling of electric water heaters under dynamic pricing. Sustainable Cities and Society. 2017;31:109-21.

[15] Luo Z, Peng J, Cao J, Yin R, Zou B, Tan Y, et al. Demand Flexibility of Residential Buildings: Definitions, Flexible Loads, and Quantification Methods. Engineering. 2022;16:123-40.

[16] Kepplinger P, Huber G, Petrasch J. Autonomous optimal control for demand side management with resistive domestic hot water heaters using linear optimization. Energy and Buildings. 2015;100:50-5.

[17] Al-jabery K, Xu Z, Yu W, Wunsch DC, Xiong J, Shi Y. Demand-Side Management of Domestic Electric Water Heaters Using Approximate Dynamic Programming. IEEE Transactions on Computer-Aided Design of Integrated Circuits and Systems. 2017;36(5):775-88.

[18] Lin B, Li S, Xiao Y. Optimal and Learning-Based Demand Response Mechanism for Electric Water Heater System. Energies. 2017;10(11).

[19] Wang J, Shi Y, Fang K, Zhou Y, Li Y. A Robust Optimization Strategy for Domestic Electric Water Heater Load Scheduling under Uncertainties. Applied Sciences. 2017;7(11).

[20] Tejero-Gómez JA, Bayod-Rújula AA. Energy management system design oriented for energy cost

optimization in electric water heaters. Energy and Buildings. 2021;243.
[21] Kapsalis V, Safouri G, Hadellis L. Cost/comfort-oriented optimization algorithm for operation scheduling of electric water heaters under dynamic pricing. Journal of Cleaner Production. 2018;198:1053-65.
[22] Tang H, Wang S, Li H. Flexibility categorization, sources, capabilities and technologies for energy-flexible and grid-responsive buildings: State-of-the-art and future perspective. Energy. 2021;219.
[23] D'hulst R, Labeeuw W, Beusen B, Claessens S, Deconinck G, Vanthournout K. Demand response flexibility and flexibility potential of residential smart appliances: Experiences from large pilot test in Belgium. Applied Energy. 2015;155:79-90.
[24] Klaassen EAM, Kobus CBA, Frunt J, Slootweg JG. Responsiveness of residential electricity demand to dynamic tariffs: Experiences from a large field test in the Netherlands. Applied Energy. 2016;183:1065-74.
[25] Lezama F, Soares J, Canizes B, Vale Z. Flexibility management model of home appliances to support DSO requests in smart grids. Sustainable Cities and Society. 2020;55.
[26] Setlhaolo D, Xia X, Zhang J. Optimal scheduling of household appliances for demand response. Electric Power Systems Research. 2014;116:24-8.
[27] Aelenei D, Lopes RA, Aelenei L, Gonçalves H. Investigating the potential for energy flexibility in an office building with a vertical BIPV and a PV roof system. Renewable Energy. 2019;137:189-97.
[28] Li H, Wang Z, Hong T, Piette MA. Energy flexibility of residential buildings: A systematic review of characterization and quantification methods and applications. Advances in Applied Energy. 2021;3.
[29] Salpakari J, Lund P. Optimal and rule-based control strategies for energy flexibility in buildings with PV. Applied Energy. 2016;161:425-36.
[30] Zhang K, Prakash A, Paul L, Blum D, Alstone P, Zoellick J, et al. Model predictive control for demand flexibility: Real-world operation of a commercial building with photovoltaic and battery systems. Advances in Applied Energy. 2022;7.
[31] Zhan S, Dong B, Chong A. Improving energy flexibility and PV self-consumption for a tropical net zero energy office building. Energy and Buildings. 2023;278.
[32] Zong Y, Mihet-Popa L, Kullmann D, Thavlov A, Gehrke O, Bindner HW. Model predictive controller for active demand side management with PV self-consumption in an intelligent building. Conference Model predictive controller for active demand side management with PV self-consumption in an intelligent building. IEEE, p. 1-8.
[33] Fotouhi Ghazvini MA, Soares J, Abrishambaf O, Castro R, Vale Z. Demand response implementation in smart households. Energy and Buildings. 2017;143:129-48.
[34] Lu Q, Yu H, Zhao K, Leng Y, Hou J, Xie P. Residential demand response considering distributed PV consumption: A model based on China's PV policy. Energy. 2019;172:443-56.
[35] Bahramara S. Robust Optimization of the Flexibility-constrained Energy Management Problem for a Smart Home with Rooftop Photovoltaic and an Energy Storage. Journal of Energy Storage. 2021;36.
[36] Gautam KR, Andresen GB. Performance comparison of building-integrated combined photovoltaic thermal solar collectors (BiPVT) with other building-integrated solar technologies. Solar Energy. 2017;155:93-102.
[37] Hou Q, Zhang N, Du E, Miao M, Peng F, Kang C. Probabilistic duck curve in high PV penetration power system: Concept, modeling, and empirical analysis in China. Applied Energy. 2019;242:205-15.
[38] Schram WL, Lampropoulos I, van Sark WGJHM. Photovoltaic systems coupled with batteries that are optimally sized for household self-consumption: Assessment of peak shaving potential. Applied Energy. 2018;223:69-81.
[39] Li Y, O'Neill Z, Zhang L, Chen J, Im P, DeGraw J. Grey-box modeling and application for building energy simulations - A critical review. Renewable and Sustainable Energy Reviews. 2021;146.
[40] Marty-Jourjon V, Goyal A, Berthou T, Stabat P. Identifiability study of an RC building model based on the standard ISO13790. Energy and Buildings. 2022;276.

[41] Florschuetz LW. Extension of the Hottel-Whillier model to the analysis of combined photovoltaic/thermal flat plate collectors. Solar Energy. 1979;22(4):361-6.
[42] Beckman. JADWA. Solar Engineering of Thermal Processes. University of Wisconsin-Madison1980.
[43] Wang C, Ji J, Zhang C, Ke W, Tang Y, Tian X. Experimental and numerical investigation of a multi-functional photovoltaic/thermal wall: A practical application in the civil building. Energy. 2022;241.
[44] Wang C, Ji J, Uddin MM, Yu B, Song Z. The study of a double-skin ventilated window integrated with CdTe cells in a rural building. Energy. 2021;215.
[45] GB 50736-2012. Design code for heating ventilation and air conditioning of civil buildings. 2012.
[46] GB 19576-2019. Minimum allowable values of energy efficiency and energy efficiency grades for unitary air conditioners. 2019.
[47] GB 50015-2019. Standard for design of building water supply and drainage. 2019.
[48] China Southern Power Grid. http://95598.csg.cn/. [Accessed 5 March 2023].
[49] Asghari M, Fathollahi-Fard AM, Mirzapour Al-e-hashem SMJ, Dulebenets MA. Transformation and Linearization Techniques in Optimization: A State-of-the-Art Survey. Mathematics. 2022;10(2).